Molecular Psychiatry
https://doi.org/10.1038/s41380-020-0720-x

ARTICLE

FAM19A5/TAFA5, a novel neurokine, plays a crucial role in depressive-like and spatial memory-related behaviors in mice

Shiyang Huang[1] · Can Zheng[2] · Guoguang Xie[3] · Zhanming Song[1] · Pingzhang Wang[1,4] · Yun Bai[5] · Dixin Chen[6] · Yan Zhang[1] · Ping Lv[1,4] · Weiwei Liang[1] · Shaoping She[1] · Qingqing Li[1] · Zhongtian Liu[1] · Yun Wang[3] · Guo-Gang Xing[3] · Ying Wang[1,4]

Received: 1 November 2019 / Revised: 16 March 2020 / Accepted: 24 March 2020

Abstract

FAM19A5/TAFA5 is a member of the family with sequence similarity 19 with unknown function in emotional and cognitive regulation. Here, we reported that FAM19A5 was highly expressed in the embryonic and postnatal mouse brain, especially in the hippocampus. Behaviorally, genetic deletion of *Fam19a5* resulted in increased depressive-like behaviors and impaired hippocampus-dependent spatial memory. These behavioral alterations were associated with the decreased expression of α-amino-3-hydroxy-5-methyl-4-isoxazolepropionic acid receptors and N-methyl-D-aspartic acid receptors, as well as significantly reduced glutamate release and neuronal activity in the hippocampus. Subsequently, these changes led to the decreased density of dendritic spines. In recent years, the roles of chronic stress participating in the development of depression have become increasingly clear, but the mechanism remains to be elucidated. We found that the levels of FAM19A5 in plasma and hippocampus of chronic stress-treated mice were significantly decreased whereas overexpression of human FAM19A5 selectively in the hippocampus could attenuate chronic stress-induced depressive-like behaviors. Taken together, our results revealed for the first time that FAM19A5 plays a key role in the regulation of depression and spatial cognition in the hippocampus. Furthermore, our study provided a new mechanism for chronic stress-induced depression, and also provided a potential biomarker for the diagnosis and a new strategy for the treatment of depression.

Introduction

Family with sequence similarity 19 (FAM19A) comprises of five highly homologous genes discovered by a novel database searching strategy, which encode secretory proteins and are found to be predominantly expressed in the central nervous system [1]. Increasing evidence has shown that FAM19A family is involved in the regulation of cognition and emotion [2, 3]. *Fam19a1* deficiency mice are

These authors contributed equally: Shiyang Huang, Can Zheng, Guoguang Xie

Supplementary information The online version of this article (https://doi.org/10.1038/s41380-020-0720-x) contains supplementary material, which is available to authorized users.

✉ Guo-Gang Xing
ggxing@bjmu.edu.cn

✉ Ying Wang
yw@bjmu.edu.cn

[1] Department of Immunology, School of Basic Medical Sciences, and NHC Key Laboratory of Medical Immunology, Peking University, Beijing 100191, China

[2] Department of Clinical Laboratory, Shanghai General Hospital, Shanghai Jiao Tong University School of Medicine, Shanghai 200080, China

[3] Neuroscience Research Institute and Department of Neurobiology, School of Basic Medical Sciences, Peking University; Key Laboratory for Neuroscience, Ministry of Education and National Health Commission, Peking University, Beijing 100191, China

[4] Center for Human Disease Genomics, Peking University, Beijing 100191, China

[5] Department of Cell Biology, School of Basic Medical Sciences, Peking University, Beijing 100191, China

[6] Drug Non-Clinical Evaluation and Research Center of Guangzhou General Pharmaceutical Research Institute, Guangzhou, Guangdong 510240, China

Published online: 21 April 2020

hyperactive and *Fam19a2* deficiency causes neuropsychiatric diseases including cognitive impairment and emotional disorders [2, 3]. FAM19A5, also termed TAFA5, is highly expressed in the hippocampus, hypothalamic paraventricular nucleus and supraoptic nuclei in the rat brain [4]. In addition, FAM19A5 plays an important role in the development of nervous system from an early stage [5]. A recent study has reported that a patient with a combination of chromosomal abnormalities including *TUSC7* gene, *FAM19A5* gene and 43 RefSeq genes microdeletions shows development delay, mood swings, hyperexcitability and sleep disturbance [6]. Our previous study has identified that sphingosine-1-phosphate receptor 2 (S1PR2) is a G protein-coupled receptor for FAM19A5 [7]. Of interest, blockade of S1PR2 signaling causes seizures, hippocampal insults, spatial memory impairment and anxiety [8]. Although FAM19A5 expression has been found to be associated with nervous system development and neurological or psychiatric disorders, the physiological and pathological functions of FAM19A5 in the emotional and cognitive regulation remain largely unknown.

A variety of studies suggest that the hippocampus is not only a cognitive structure associated with learning and memory, but also a mood regulator whose dysfunction can lead to mental disorders [9–11]. Over the past 20 years, depression has become increasingly recognized as the important component of emotional dysfunction [12]. Depression is a chronic mental disorder, which is characterized by several persistent symptoms, including depressed mood, anhedonia, irritability, and mental retardation [13, 14]. Environmental stressors play important roles in the development and progression of depression, leading to stable changes in gene expression, neural circuit function and ultimately behaviors [15–17]. In dysregulated stress responses, dysfunction of glutamate, norepinephrine and cytokine may lead to dendritic structure disorder, neuronal apoptosis, and altered hippocampal neurogenesis [16, 18–20]. A lot of studies have established a robust and causal association between stressful life events and depression, yet the molecular mechanism by which stress induces depression is not well understood.

Here, we demonstrated for the first time to our knowledge that FAM19A5 ablation caused deficiency in dendritic spine morphology, glutamate signaling, and neuronal activity, subsequently leading to depressive-like behaviors and cognitive impairment in mice. FAM19A5 was decreased in plasma and hippocampus in mice subjected to chronic stress. Human FAM19A5 overexpression in hippocampus mediated antidepressant-like effects in chronic stress-treated mice. Our study suggested that FAM19A5 may be an attractive target for new antidepressants.

Materials and methods

Animals

The genetic background of all mice is C57BL/6 J. The mice were housed and bred under specific pathogen-free conditions at the Health Science Center, Peking University. All animal experiments were performed in accordance with the guidelines of the National Institutes of Health Guide for the Care and Use of Laboratory Animals and approved by the Ethics Committee of Peking University Health Science Center. All data derived from animal studies were analyzed by an experimenter blind to experimental conditions. The order of the animals was further randomized prior to behavioral tests.

Generation of *Fam19a5* knockout mice

Fam19a5$^{-/-}$ mice were generated on a C57BL/6 J background by CRISPR/Cas9-mediated gene targeting. We designed target guide RNA specific to exon 2 of *Fam19a5*, which was microinjected into the fertilized eggs of C57BL/6 J mice. Integration of the targeting construct was confirmed by Southern blot. Targeted embryonic stem cell lines were injected into C57BL/6 J blastocysts. Heterozygous matings were set up to generate homozygous mutant mice. Genomic DNA was extracted from tail biopsies for PCR genotyping and sequencing. The primer sequences for the PCR were as follows: primer 1, 5′-ACCTGTGAGATT GTGACCCT-3′; primer 2, 5′- CTTGCCTGCTCACACA GAAAC-3′; 94 °C for 30 s, 60 °C for 30 s, and 72 °C for 40 s. The targeted allele yielded a DNA fragment of about 180 bp and the wild-type allele yielded a fragment of about 210 bp.

Protein and antibody

Recombinant FAM19A5 was obtained as previously described [7]. The rabbit polyclonal antibody for FAM19A5 was obtained and purified as previous protocol [7]. Commercial antibodies used were: goat anti-FAM19A5 (R&D, AF5148), mouse anti-NeuN (Millipore, MAB377), rabbit anti-NeuN (Abcam, ab128886), mouse anti-GFAP (Cell Signaling Technology, 3670 T), mouse anti-Nestin (Abcam, ab6320), rabbit anti-VGLUT2 (Invitrogen, 42-7800), rabbit anti-Iba1 (Wako, 019-19741), rabbit anti-Olig2 (Abcam, ab109186), mouse anti-GAD67 (Millipore, MAB5406) and rabbit anti-Flag (Abcam, ab1162).

Plasma and cerebrospinal fluid (CSF) collection

Mice were anesthetized with avertin (240 mg/kg), eyeballs were removed, and EDTA was used as anticoagulant to

collect blood rapidly. Plasma was collected after centrifugation at 3000 × *g* for 5 min.

CSF was sampled as previously described [21]. Briefly, mice were anesthetized by intraperitoneal (i.p.) injection of pentobarbital sodium (50 mg/kg) and placed into a stereotaxic apparatus (RWD Life Science). CSF was collected from the lateral ventricle (Bregma anteroposterior (AP): −0.94 mm, mediolateral (ML): ± 1.60 mm, dorsoventral (DV): −2.00 mm). CSF was withdrawn at a rate of 0.2 μL/min, under the control of a micro-syringe pump to obtain a volume of 3–4 μL. CSF was collected after centrifugation at 3000 × *g* for 5 min.

Cytometric bead assay of mouse FAM19A5

Aldehyde/sulfate latex microspheres (100 μL; Invitrogen) and rabbit anti-FAM19A5 polyclonal antibody (20 μL; 2.5 mg/mL) were mixed in 200 μL 2-morpholinoethanesulfonic acid buffer (0.025 M, pH = 6.0). The complex was then incubated at 4 °C overnight, and the microspheres coated with FAM19A5 polyclonal antibody were processed according to the Latex Bead Protein Coupling Protocols (Invitrogen). Plasma or tissue lysates extracted with PBS were cleared by centrifugation at 12,000 × *g* for 5 min at 4 °C. Total protein concentration was measured by using Pierce BCA Protein Assay Kit (Thermo Fisher Scientific). 20 μL plasma was then diluted 2000 times and tissue lysates were diluted with a final concentration at 1 mg/mL. For comparison of plasma and CSF, 2 μL plasma and CSF were diluted 2,000 times. For the standard curve, 0, 10, 20, 40, 80, 160, 320, 640, 1250, 2500, 5000, or 10,000 pg/mL dilutions of FAM19A5 in 50 μL 5% bovine serum albumin (BSA; Roche)/PBS buffer were prepared.

After blocking microspheres in 5% BSA/PBS buffer for 30 min, 50 μL tissue lysates, plasma or CSF and 2 μL microspheres were mixed and incubated for 2 h at room temperature. Supernatant was removed after centrifugation at 3000 × *g* for 5 min at 4 °C. Microspheres were then incubated with 50 μL goat anti-FAM19A5 at 1 mg/mL in 5% BSA/PBS buffer for 1 h. Supernatant was then removed after centrifugation at 3000 × *g* for 5 min at 4 °C, followed by incubation in 50 μL PE anti-goat IgG (eBioscience) at a dilution of 1:1000 in PBS buffer for 30 min. After removal of the supernatant, microspheres were resuspended in 300 μL PBS and analyzed by FACS Verse (BD Biosciences).

Reverse transcription PCR and quantitative real-time PCR (qPCR)

Total RNA was extracted and purified from fresh mouse tissues or cultured cells using Trizol Reagent (Life Technologies), then equal amounts (2 μg) were reverse-transcribed to cDNA. After the reverse transcription step (25 °C for 5 min, 42 °C for 50 min, 85 °C for 5 min), the cDNA of interest was amplified by 30 PCR cycles and analyzed on 1% agarose gel. The sequences of the primers used for PCR amplification were listed in Supplementary Table 1.

SYBR Green 2× PCR Mastermix (Yeason) was used according to the manufacturer's instructions. The PCR program consisted of 95 °C for 5 min; 40 cycles of 95 °C for 10 s, 60 °C for 30 s, and 72 °C for 30 s; and 72 °C for 5 min. Quantitative real-time PCR amplification was performed by using Mx3000P Real-Time PCR System (Agilent StrataGene). The expressions of candidate genes were normalized to GAPDH.

Histological analysis and immunohistochemistry

Mice were anesthetized with avertin (240 mg/kg) and perfused transcardially with ice-cold PBS, followed by 4% paraformaldehyde (PFA) in PBS. Brains were post-fixed in 4% PFA overnight at 4 °C and dehydrated in 20 and 30% sucrose in PBS subsequently for frozen sections, or dehydrated in 60, 70, 80, 90, 100% ethanol and dimethylbenzene subsequently for paraffin sections.

For histological analysis, tissue paraffin sections were pretreated at 65 °C for 4 h and then hydrated in 100, 95, 90, 80, and 70% ethanol, then stained with hematoxylin and eosin. For immunohistochemistry, tissue paraffin sections were pretreated at 65 °C for 4 h and then hydrated in 100, 95, 90, 80, and 70% ethanol. The antigens were retrieved by the high-pressure method, and peroxidase was removed by incubating the sections in 3% H_2O_2 for 20 min. After sections were blocked by goat serum in working buffer for 1 h, primary antibody or species-matched IgG was applied onto the sections at 4 °C overnight followed by appropriate secondary HRP-conjugated antibody before staining with DAB Kit (ZSGB-BIO, ZLI-9018). Nuclei were counterstained with hematoxylin. For multiplex immunohistochemistry, after sections were blocked by goat serum in working buffer for 1 h, rabbit anti FAM19A5 (10 μg/mL) was applied onto the sections at 4 °C overnight followed by appropriate secondary HRP-conjugated antibody. Then applied 100–400 μL Alexa Fluor 568-conjugated Tyramide Signal Amplification plus amplification reagent (Invitrogen, B40956) per slide and incubated for 10 min at room temperature. The antigens were retrieved by the high-pressure method and blocked by goat serum. Rabbit anti-VGLUT2 antibody (1:200), rabbit anti-Iba1 antibody (1:100) or rabbit anti-Olig2 antibody (1:200) was applied onto the sections at 4 °C overnight. After goat antirabbit IgG conjugated with Alexa Fluor 488 (1:200; Invitrogen, A11070) were utilized as secondary antibodies for 1 h at room temperature, the tissue sections were counterstained with DAPI (Sigma, 1 μg/mL) for 20 min at room temperature. Slices were mounted with Fluorescence Mounting Medium (Dako) and imaged.

Immunofluorescent staining

Tissue paraffin sections or frozen sections were blocked by goat serum in working buffer for 1 h, then 5 μg/mL rabbit anti-FAM19A5 antibody, mouse anti-Nestin antibody (1:200), mouse anti-NeuN antibody (1:500), mouse anti-GFAP antibody (1:500), mouse anti-GAD67 antibody (1:200) or rabbit anti-Flag antibody (1:100) was applied onto the sections at 4 °C overnight. After the tissue sections were washed five times in PBS buffer, goat antimouse or antirabbit IgG conjugated with either Alexa Fluor 488 (1:200; ZSGB-BIO, ZF-0512) or 594 (1:200; ZSGB-BIO, ZF-0516) was utilized as secondary antibodies for 1 h at room temperature. The tissue sections were washed five times in PBS buffer and counterstained with DAPI for 20 min at room temperature. Slices were mounted with Fluorescence Mounting Medium and imaged.

Cultures for neurosphere, primary cortical neurons and astrocytes

Neurosphere cultures were prepared from embryonic day 16.5 C57BL/6 J mouse brains as described [22]. Mouse forebrains were isolated from the embryos for cell preparation. Embryonic brains were minced and digested with 0.5% accutase (Gibco-BRL) at 37 °C for 30 min. After washed with PBS buffer twice, cells were cultured in serum-free Dulbecco's Modified Eagle Medium (DMEM)/F12 medium (Gibco-BRL) supplied with 2% B27 supplement (Gibco-BRL) and 20 ng/mL mouse fibroblast growth factor/epidermal growth factor (EGF) (Peprotech). Cells were maintained at 37 °C in 5% CO_2 to obtain the primary neurospheres.

Primary cortical neuron cultures were prepared from embryonic day 16.5 C57BL/6 J mouse brains as described [23]. Cells were plated on coverslips coated with poly-D-lysine (1 mg/mL) at a density of 100,000/coverslip. Neurons were cultured in neurobasal medium supplemented with 2% B27 (Gibco-BRL), 1% glutamax (Gibco-BRL) at 37 °C in a humidified atmosphere of 5% CO_2. Thereafter, one third to half of the medium was replaced every 3 days.

Primary astrocyte cultures were prepared from the cortex of C57BL/6 J mouse pups (postnatal days 0–3) as described [24, 25]. The animals were euthanized with an overdose of isoflurane (RWD Life Science), the forebrains were dissected out. Cortex cuts from two animals were used for each cell culture preparation. After separation, the cells were plated on poly-D-lysine-coated glass coverslips and cultured in DMEM/F12 medium supplied with 10% fetal bovine serum (Gibco-BRL) and 1% penicillin/streptomycin (Gibco-BRL) at 37 °C in 5% CO_2. Thereafter, one third to half of the medium was replaced every three days.

Behavioral studies

All behavioral experiments were conducted blind with the treatment and genotype of the mice. Only 2- to 3-month-old male mice were used for behavioral testing.

Open field test

Mice were free to explore in a plastic open-field chamber (40-cm width × 40-cm length × 30-cm height), recorded by Smart 3.0 video tracking system. Mice were individually placed in the center of the arena and allowed to move freely in the arena for 30 min. Total distance traveled in 30 min and time spent in the center region (20 cm × 20 cm) in the first 5 min was recorded.

Elevated plus maze test

The elevated plus maze apparatus contained a 6 × 6 cm center square, two closed and two open arms at 35 × 6 cm^2 each, orthogonally arranged 60 cm above the ground. Closed arms were surrounded by 20-cm height black walls. Mice were placed on the center platform, facing an open arm and allowed to freely explore it for 5 min. Traveled total distance, numbers of open arm entries and percentage of time in the open arms were measured. Data were recorded and analyzed using Smart 3.0 video tracking system.

Sucrose preference test

Mice were housed individually and acclimatized to 1% sucrose solution (w/v) or sterilized tap water in two bottles. After 24 h, mice were allowed free access to two bottles contained 1% sucrose solution or sterilized tap water. To avoid bottle side preference, the positions of the two bottles were swapped. The weights of liquid in the two bottles were measured and sucrose preference was defined as: sucrose preferences (%) = sucrose consumption/(sucrose + water consumption) ×100%.

Forced swimming test

Mice were individually placed in a transparent acrylic cylinder (20 cm in diameter, 40 cm in height) filled with 30 cm height of water maintained at 22 °C. Mice were placed in the water for 6.5 min using a video tracking system (Smart 3.0). The time mice spent immobile was analyzed during the final 5 min of test.

Tail suspension test

Mice were suspended by their tails with adhesive tape for 6.5 min and videotaped with Smart 3.0 video tracking

system. The time mice spent immobile during the final 5 min of suspension period was recorded.

Morris water maze test

The water maze used in this study comprised a circular tank with a diameter of 120 cm and a depth of 60 cm. The tank was filled with opaque water at a temperature of 22 ± 2 °C and equipped with a transparent escape platform with a diameter of 10 cm, which was located 1 cm below the water surface. Different visual clues were pasted around the tank, which served as spatial landmarks for the mouse. A video camera was installed above the maze to record the swimming traces in the water maze. The water maze was divided into four quadrants, the target quadrant (the one previously containing the platform), and three nontarget quadrants (opposite quadrant, adjacent right, and adjacent left). On day 0, mice were trained to find the platform with a visible flag. On days 1–6, the platform was submerged 1–2 cm below the water surface. Mice were placed into the maze at one of four quadrants, facing the wall of the tank, and searched for the platform for 60 s. If a mouse failed, it was guided to the platform and maintained for 15 s. Four trials a day were conducted with a 45-min interval between trials. Escape latency was recorded. Spatial memory test was performed on day 7 with the platform removed, occupancy time (%) in the target quadrant was compared with all other quadrants and the platform crossings in the target quadrant were compared with a similar area in all other quadrants.

Mouse models of chronic stress

Chronic restraint stress model

Naive 8-week-old male C57BL/6 J mice were subjected to chronic restraint stress (CRS) for 2–3 h per day for 14 consecutive days by placement into 50-mL conical tubes with three holes for air flow and allowed to stretch their legs but not to move within the tube [26, 27]. Naive age-matched not-stressed animals were used as controls.

Chronic forced swimming stress model

Naive 8-week-old male C57BL/6 J mice were subjected to chronic forced swimming stress (CFSS) for 5 min per day for 5 consecutive days by placement into a transparent acrylic cylinder filled with 30 cm height of water. Naive age-matched not-stressed animals were used as controls.

Chronic social defeat stress model

Chronic social defeat stress was performed according to previously protocol [28]. Test 8-week-old male C57BL/6 J mouse was directly placed into the cage side of male CD-1 retired breeder mouse at 4–6 months of age for 5–10 min of social defeat per day for up to 10 days. After direct interaction with the CD-1 aggressor, the C57BL/6 J mouse was transferred to the opposite side of the perforated divider and placed in the divider chamber for 24 h with sensory but no physical contact. For the control group, C57BL/6 J mice pairs were placed in equivalent cages with sensory without any physical contact. The mice were rotated between control cages every day. Twenty-four hours after the last social defeat, social interaction tests were performed. C57BL/6 J mice were habituated to behavioral testing suite 1 h before social interaction test. For the social interaction test in the first 2.5 min trial ("no target"), the C57BL/6 J defeated mouse was placed into the social interaction arena and allowed to explore freely an open-field arena (40 × 40 cm) possessing an empty wire-mesh cage (10 × 6 cm) without a "target" CD-1 mouse. During the second 2.5 min trial ("target"), the mouse was reintroduced into this arena to move freely in the presence of the "target" CD-1 mouse. Smart 3.0 Video tracking system was used to record and analyze time spent in the "corner zone" (9 × 9 cm) and "interaction zone" (12 × 25 cm). Social interaction ratio refers to the ratio of time spent in the "interaction zone" to time spent in the "corner zone." Resilience group refers to social interaction ratio ≥1 and susceptible group refers to social interaction ratio <1.

Bioinformatic analyses of RNA-sequencing data

Total RNA was extracted from the whole hippocampus using TRIzol Reagent according the manufacturer's instructions (Invitrogen). RNA quality was then measured by using 2100 Bioanalyser (Agilent) and quantified using the ND-2000 (NanoDrop Technologies). Only high-quality RNA sample (OD260/280 = 1.8–2.2, OD260/230 ≥ 2.0, RIN ≥ 6.5, 28 S:18 S ≥ 1.0, >10 μg) was used to construct sequencing library. RNA-seq transcriptome library was prepared following TruSeqTM RNA sample preparation Kit from Illumina (San Diego, CA) using 5 μg of total RNA. The data were analyzed on the free online platform of Majorbio I-Sanger Cloud Platform (www.i-sanger.com). Sequencing was performed on an Illumina Platform with 150 paired end reads. Each sample had 48–56 M clean reads and Q30 > 93%. Clean data (reads) was alignment with the reference whole genome with samples having >97% mapped reads. The sequencing data from this study can be found at NCBI sequence read archive under accession PRJNA601747. To identify DEGs (differential expression genes) between two different samples, the expression level of each transcript was calculated according to the fragments per kilobase of exon per million mapped reads method. RSEM was used to quantify gene abundances. R statistical

package software empirical analysis of digital gene expression in R (EdgeR) was utilized for differential expression analysis. In addition, to identify which DEGs were significantly enriched in metabolic pathways, functional-enrichment analyses including Kyoto encyclopedia of genes and genomes (KEGG) were performed at Bonferroni-corrected P value ≤ 0.05 compared with the whole-transcriptome background. And gene set enrichment analysis (GSEA) was performed (http://www.broadinstitute.org/gsea/index.jsp) on *Fam19a5*$^{-/-}$ vs WT differential expression genes data of hippocampal samples.

Sparse labeling and dendritic spine density analysis

Sparse labeling was performed according to previously described [29, 30]. The mice were anesthetized by i.p. injection of pentobarbital sodium. The Adeno-associated viruses (AAVs) containing rAAV-EF1α-DIO-EGFP (BrainVTA, PT-0795) and rAAV-CaMKIIα-Cre (BrainVTA, PT-0220) were injected into the hippocampal CA1 region (Bregma AP: −2.06 mm, ML: ± 1.50 mm, DV: −1.30 mm). After 3 weeks, the brains were extracted, fixed in 4% PFA overnight at 4 °C, and dehydrated in 20 and 30% sucrose in PBS buffer. Consecutive 80 μm coronal brain slices were washed with PBS for 3 times. Dendritic spines in hippocampal CA1 region were visualized by a confocal microscope (TCS SP8 STED, Leica, Germany), using a 60× oil-immersion objective. For dendritic spine morphological analysis, Z-stacks consisted of 20 scans at 0.3-μm intervals to image the entire thickness of the dendrite. Dendritic spines were counted along dendritic segments that were chosen from secondary and tertiary dendrites. Dendritic spines with a neck could be classified as either thin or mushroom, and those without an apparent neck are classified as stubby. Dendritic spines with a neck are labeled as thin or mushroom according to head diameter. Results were expressed as spine density/μm.

Fiber photometry recording in mice during behavioral tests

The mice were anesthetized by i.p. injection of pentobarbital sodium and placed into a stereotaxic apparatus. Fiber photometry experiments were performed as previously described [31]. The AAVs containing rAAV-EF1α-DIO-GCaMP6s (BrainVTA, PT-0071) and rAAV-CaMKIIα-Cre were injected into the hippocampal CA1 region (Bregma AP: −2.06 mm, ML: ± 1.50 mm, DV: −1.30 mm) of C57BL/6 J mice in a volume of 300 nL at 60 nL/min. For glutamate measurement experiments performed as previously described [32], the AAVs containing rAAV-EF1α-DIO-iGluSnFR (A184S)-WPRE-hGHpolyA (BrainVTA, PT-1142) and rAAV-CaMKIIα-Cre were injected into the hippocampal CA1 region of C57BL/6 J mice in a volume of 300 nL at 60 nL/min. An optic fiber (200 μm O.D., NA = 0.37, Shanghai Fiblaser) housed in a ceramic ferrule (Shanghai Fiblaser) was implanted 0.1 mm above the injection site. One week after virus injection, a fiber photometry system (Thinker Tech, Nanjing) was used for recording fluorescence signal which produced by an exciting laser beam from a 490 nm laser. For recordings of CA1 excitatory neuron activities during stress, mice were suspended by their tails for 5 min. Post hoc histology was used to confirm the expression of GCaMP6s or iGluSnFR and the correct placement of optic fibers. Photometry data were exported from CamFiberPhotometry to MATLAB mat files for further analysis. Data were segmented according to behavioral events within individual trials. Fluorescence change (ΔF/F) was calculated by (F-F0)/(F0-F_{offset}), where F0 refers to the median of the fluorescence values during the baseline period and F_{offset} refers to the fluorescence values of environment. The ΔF/F values were presented with per-event plots with shaded areas indicating s.e.m. or heatmaps.

AAV-FAM19A5 construction and injection

The adeno-associated virus (AAV)-9 delivery system that overexpressed the human *FAM19A5* gene (AAV9-hSyn-FAM19A5) in mouse brain was constructed by Vigene Biosciences (Shangdong, China). The C-terminal of *FAM19A5* gene on the vector expressed the Flag tag. The empty (AAV9-hSyn-Null) served as a control. Titers of the vector genome were measured by quantitative reverse-transcription PCR with vector-specific primers. Viruses containing 1 × 10^13 AAV9 vector genomes were injected into the hippocampal CA1 region (Bregma AP: −2.06 mm, ML: ± 1.50 mm, DV: −1.30 mm) of naive 8-week-old male C57BL/6 J mice in a volume of 500 nL at 100 nL/min. Three weeks after virus injection, mice were subjected to CRS for 2–3 h per day for another 10 days.

Statistical analysis

All quantitative biochemical data were representative of three independent experiments, and all behavioral data were representative of at least two experiments. Statistical analysis was performed using GraphPad prism 8.0 software (GraphPad Software, San Diego, CA, USA). Animal exclusion according to identify outliers (ROUT method) of GraphPad prism 8.0 software was not made for data analyses. For statistical comparisons, whether data were Gaussian distribution was first evaluated. The data were normally distributed and variances were similar between groups to be compared, therefore parametric statistical tests were justified and used. When the data were not normal distribution, we performed nonparametric statistical tests.

Statistical significance was determined using the two-tailed Student's *t* test (unpaired) for comparison between two groups. Statistically significant differences between groups were determined using one-way ANOVA with Dunn's multiple comparisons. For multiple comparisons, two-way ANOVA with Sidak's multiple comparison tests were used. All experiments were performed at least three independent experiments. All data were represented as the mean ± s.e.m., and the significant differences between groups were represented by $*0.01 < P < 0.05$, $**0.001 < P < 0.01$, and $***P < 0.001$, ns, no significance.

Results

Expression of FAM19A5 in the embryonic and postnatal mouse brain

To investigate the expression profile of FAM19A5, we detected the levels of FAM19A5 in several adult wild-type (WT) mouse tissues and embryo by qPCR and cytometric bead array (CBA) as previously described [7]. As shown in Fig. 1a, b, FAM19A5 mRNA and protein were highly expressed in the brain, with mild to moderate expression in the eye, embryo and heart, and were barely detectable in other tissues. We then measured the concentration of FAM19A5 in plasma and CSF of adult WT mouse. The result of CBA showed that the expression of FAM19A5 in the mouse CSF was approximately the same as that in the plasma (Fig. 1c). Next, we detected the expression levels of FAM19A5 during the brain development. As shown in Fig. 1d, e, the expression of FAM19A5 was gradually increased from embryonic day (E) 12.5 to postnatal day (P) 1, peaked at P 1 for mRNA and P 7 for protein, and was decreased at postnatal week 8, suggesting that FAM19A5 may be involved in the brain development. Furthermore, we determined the expression patterns of FAM19A5 in some brain regions including cerebral cortex, amygdala, hippocampus, hypothalamus, thalamus and cerebellum by qPCR and CBA. As shown in Fig. 1f, g, FAM19A5 mRNA and protein were abundantly expressed in the hippocampus compared with other brain regions. To further verify the locations of FAM19A5 in the brain, an immunohistochemical assay was performed using the rabbit polyclonal antibody against FAM19A5 as previously described [7]. The results also demonstrated that FAM19A5 was abundantly expressed in hippocampus, particularly in the pyramidal neurons, while moderately expressed within other regions of adult mouse brain (Fig. 1h).

To explore the molecular and cellular basis for the function of FAM19A5, we first examined the expression of FAM19A5 on several different cells in the embryonic and adult hippocampus. The results of immunofluorescent staining demonstrated that FAM19A5 was coexpressed with both NeuN, a marker of neurons, and Nestin, a marker of NSCs (Fig. 1i; Supplementary Fig. S1A), but not with GFAP, a marker of astrocytes (Supplementary Fig. S1B). Moreover, as shown in Supplementary Fig. S1C, D, FAM19A5 was coexpressed with Olig2 (a marker of oligodendrocytes) rather than Iba1 (a marker of microglia), indicating that FAM19A5 was mainly expressed in neurons, NSCs and oligodendrocytes. Next, we observed the expression of FAM19A5 in the different types of neurons, including glutamatergic neurons and GABAergic neurons. As shown in Supplementary Fig. S1E, F, FAM19A5 was coexpressed with VGLUT2 (a marker of glutamatergic neurons) rather than GAD67 (a marker of GABAergic neurons), indicating that FAM19A5 was mainly expressed in glutamatergic neurons. Then, we separated primary neurons and NSCs from embryonic brains of mice and demonstrated the expression of FAM19A5 in neurons and NSCs using cell immunofluorescent staining, qPCR and CBA (Fig. 1j–l). Data from qPCR and CBA revealed that FAM19A5 was highly expressed in HEK293T cells transfected with FAM19A5 while almost not expressed in those cells transfected with pcDNA3.1B (pcDB) empty vector (Supplementary Fig. S1G, H). Therefore, these results suggested that FAM19A5 may be associated with the function of central nervous system.

Depressive-like behaviors and spatial memory impairment in *Fam19a5* deficiency mice

To explore the physiological function of FAM19A5 in vivo, we constructed a CRISPR/Cas9-mediated targeting vector to delete gccagccacggaggacgatcgcccggcagacagc bases and mutate cacg bases in exon 2 of *Fam19a5* gene. We found that FAM19A5 was indeed undetectable in the brains of $Fam19a5^{-/-}$ mice (Supplementary Fig. S2A–C). Surprisingly, although $Fam19a5^{-/-}$ mice showed significantly decreased in both of the body and brain weights compared with the WT littermates, the brain to body weight ratio was significantly increased (Supplementary Fig. S3A–D). Also, the results from histological analysis and immunohistochemical staining of $Fam19a5^{-/-}$ mouse brain slices revealed the changes in the gross morphology of the brain (Supplementary Fig. S3E, F). Next, we investigated the behaviors of emotion and spatial cognition in $Fam19a5^{-/-}$ (KO) mice and WT littermates. We first conducted the open field test, which measures the activity and the time animals spend in the center or periphery of an open chamber. The results showed that $Fam19a5^{-/-}$ mice were more active than WT controls within the total 30 min of the assessment while spent less time in the center of the chamber (Fig. 2a–d), revealing that $Fam19a5^{-/-}$ mice exhibited a significant increase in anxiety/depressive-like behaviors

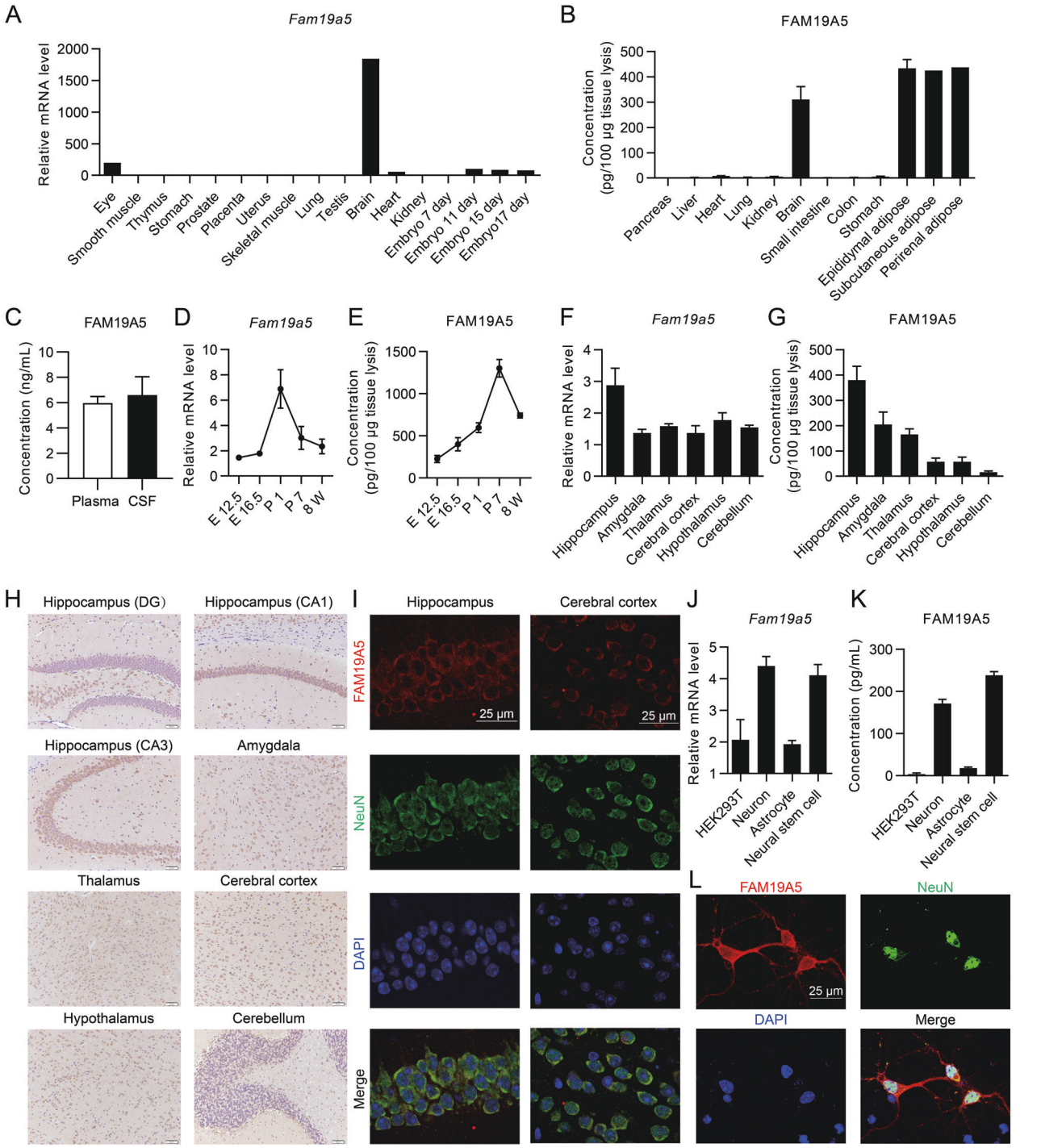

Fig. 1 Expression of FAM19A5 in the embryonic and postnatal mouse brain. a Quantitative real-time PCR (qPCR) and **b** cytometric bead analysis of FAM19A5 expression levels in mouse tissues. **c** Cytometric bead analysis of FAM19A5 expression levels in plasma and cerebrospinal fluid of adult mice. **d** qPCR and **e** cytometric bead analysis of FAM19A5 expression levels during brain development. **f** qPCR and **g** cytometric bead detection of mouse FAM19A5 in the hippocampus, amygdala, thalamus, cerebral cortex, hypothalamus, and cerebellum. **h** Immunohistochemical staining with FAM19A5 in the mouse hippocampus (DG, CA1, CA3), amygdala, thalamus, cerebral cortex, hypothalamus, and cerebellum. Scale bar = 50 μm. **i** Immunofluorescent staining with FAM19A5 and NeuN in the hippocampus and cerebral cortex. Scale bar = 25 μm. **j** qPCR detection of FAM19A5 mRNA expression levels and **k** the cytometric bead detection of FAM19A5 in the supernatant of HEK293T, primary cultured neurons, astrocytes and neural stem cells. **l** Immunofluorescent staining with FAM19A5 and NeuN in the primary cultured neurons. Scale bar = 25 μm.

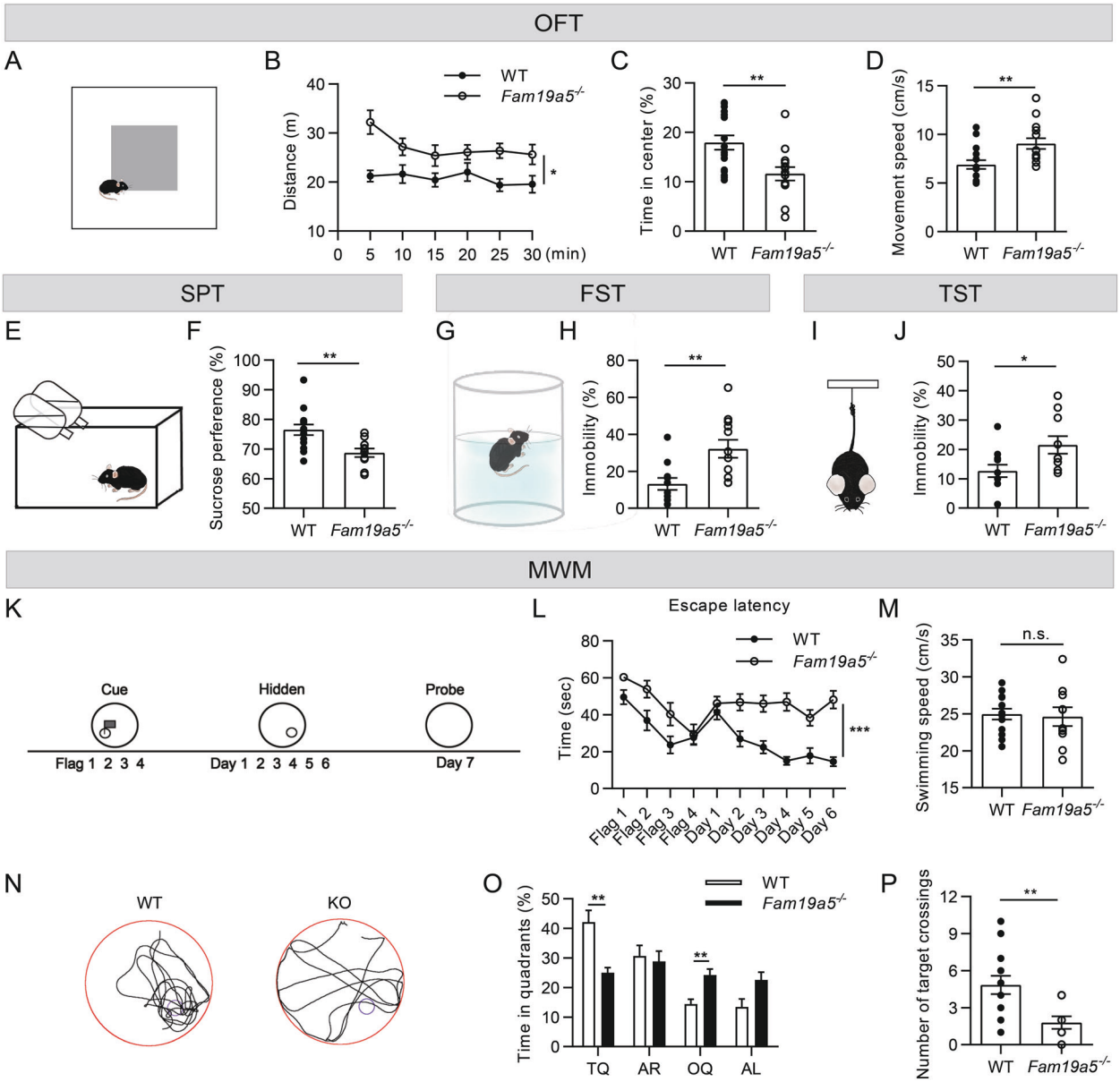

Fig. 2 Depressive-like behaviors and spatial memory impairment in *Fam19a5*$^{-/-}$ mice. a–d Open field test (OFT). **a** Diagram of open field test. **b** Distance traveled during 5 min intervals in the OFT (two-way ANOVA with Sidak's multiple comparisons test; $^{*}P < 0.05$), **c** the percentage of time spent in the central zone (unpaired two-tailed Student's t test, $t = 3.119$, $P = 0.0042$) and **d** movement speed (unpaired two-tailed Student's t test, $t = 3.040$, $P = 0.0051$) compared between WT ($n = 16$) and *Fam19a5*$^{-/-}$ ($n = 14$) mice. **e–f** Sucrose preference test (SPT). **e** Diagram of sucrose preference test. **f** The percentage of sucrose preference (unpaired two-tailed Student's t test, $t = 3.139$, $P = 0.0048$) compared between WT ($n = 14$) and *Fam19a5*$^{-/-}$ ($n = 10$) mice. **g–h** Forced swimming test (FST). **g** Experimental setup for forced swimming test. **h** The percentage of immobility time (unpaired two-tailed Student's t test, $t = 3.193$, $P = 0.0044$) compared between WT ($n = 11$) and *Fam19a5*$^{-/-}$ ($n = 12$) mice. **i–j** Tail suspension test (TST). **i** Experimental setup for tail suspension test. **j** The percentage of immobility time (Mann–Whitney test, $P = 0.0485$) compared between WT ($n = 12$) and *Fam19a5*$^{-/-}$ ($n = 10$) mice. **k–p** Morris water maze (MWM). **k** Diagram of Morris water maze test. **l** The escape latency time during training period (two-way ANOVA with Sidak's multiple comparisons test; $^{***}P < 0.001$) compared between WT ($n = 13$) and *Fam19a5*$^{-/-}$ ($n = 10$) mice. **m** Swimming speed on day 7 (unpaired two-tailed Student's t test, $t = 0.2444$, $P = 0.8093$) between the two groups of mice. **n** Representative swimming paths during the test period. **o** Time distribution in the four quadrants during the test period (two-way ANOVA with Sidak's multiple comparisons test, $^{**}P < 0.01$, $P_{TQ} = 0.0045$, $P_{OQ} = 0.0056$) and **p** number of crossing the target platform position (Mann–Whitney test, $P = 0.0028$) compared between the two groups of mice. TQ, target quadrant (where the platform was located during the training); AR, adjacent quadrant right; OQ, opposite quadrant; AL, adjacent quadrant left. All data are expressed as mean ± s.e.m.

compared with the control mice. We then performed the elevated plus maze test, a classic method for evaluating anxiety-like behavior. The results showed that there were no differences between *Fam19a5*$^{-/-}$ mice and WT control mice in the time spent in open arms and the entries into open arms, suggesting that the absence of FAM19A5 had no effect on anxiety-related behavior in mice (Supplementary Fig. S4A–C). In addition, we explored whether *Fam19a5*$^{-/-}$ mice exhibit a depressive-like phenotype by using sucrose preference test, forced swimming test and tail suspension test. We first performed sucrose preference test, which is a measurement of anhedonia, a lack of interest in reward stimuli and a manifestation of depression. The results showed that *Fam19a5*$^{-/-}$ mice had a significantly lower preference for sucrose solution than WT control mice (Fig. 2e, f), indicating increased anhedonia behavior in KO mice. We then performed forced swimming test as an acute stress assay to measure immobility time which correlates with the level of depression. *Fam19a5*$^{-/-}$ mice exhibited more despair behavior as indicated by more time of immobility than WT counterparts (Fig. 2g, h), which was also confirmed by the tail suspension test (Fig. 2i, j), an alternative acute stress assay.

The hippocampus is thought to be important for learning and memory, the behavioral responses to stress, and the pathophysiology of mood disorders [33]. Considering the high expression of FAM19A5 in hippocampus, we further assessed the hippocampus-dependent spatial learning and memory in *Fam19a5*$^{-/-}$ mice by Morris water maze (MWM) task (Fig. 2k). In the MWM test, *Fam19a5*$^{-/-}$ mice displayed significantly longer latency to find the hidden platform during the training session as compared with WT counterparts, yet no significant change in motivation in the training period during which the platform was visible to the mice (Fig. 2l). Furthermore, no difference was found between WT and *Fam19a5*$^{-/-}$ mice in their movement speed to find the platform (Fig. 2m), indicating that the apparent learning and memory deficit in the *Fam19a5*$^{-/-}$ mice was not related to deficits in vision, motivation or movement. On the day 7 probe trial with the platform removed, the *Fam19a5*$^{-/-}$ mice spent significantly less time in the target quadrant than their WT littermates (Fig. 2n, o). In addition, *Fam19a5*$^{-/-}$ mice crossed the platform area less compared with WT mice (Fig. 2p), further suggesting a deficit in spatial learning and memory.

Decreased FAM19A5 participated in the chronic stress-induced depression

Since *Fam19a5* deficiency can lead to depressive-like behaviors, we investigated whether FAM19A5 expression was changed under depression condition. Chronic stress mouse models are thought to be a more realistic mirror of human depression [34]. Mice were subjected to CRS, CFSS, and chronic social defeat stress (CSDS), three ethologically validated models of stress. First, we exposed adult wild-type mice to CRS and CFSS (Fig. 3a, b), which exhibited depressive-like behavior as indicated by more immobility time than control mice in both forced swimming test and tail suspension test (Supplementary Fig. S5A, B). After the last restraint or forced swimming in CRS or CFSS, mice were sacrificed, plasma was collected, and then hippocampus, hypothalamus, and amygdala were extracted from the brain tissues. The levels of FAM19A5 were examined by qPCR and CBA. CRS and CFSS led to significant decreased levels of FAM19A5 in the plasma (Fig. 3c) and hippocampus (Fig. 3d, e), whereas the downregulation of FAM19A5 was not observed in the amygdala (Supplementary Fig. S6A, B) and the hypothalamus (Supplementary Fig. S6C, D), two other brain regions implicated in depression. We then exposed adult wild-type mice to CSDS (Fig. 3f). After the last social defeat in CSDS, mice were tested in the social interaction test and classified into susceptible and resilient populations according to the social interaction ratio (Supplementary Fig. S7A–C). To investigate whether FAM19A5 expression in the plasma and hippocampus was altered by CSDS, we quantified FAM19A5 mRNA and protein levels in mice 24 h after the social interaction test. Compared with control and resilient mice, the susceptible mice exhibited significantly reduced levels of FAM19A5 in the plasma (Fig. 3g), which was consistent with the results of CRS and CFSS. However, the mRNA level of FAM19A5 in the hippocampus of susceptible mice was only slightly decreased (Fig. 3h). In addition, the protein level of FAM19A5 in the hippocampus of susceptible mice was significantly decreased (Fig. 3i). Similarly, the reduction of FAM19A5 was not observed in the amygdala (Supplementary Fig. S8A, B) and hypothalamus (Supplementary Fig. S8C, D).

Our previous study has reported that the amino acid sequence of FAM19A5 is quite conserved among eukaryotic species with 99.2% protein identity between the human and mouse sequences [7]. Therefore, we investigated whether human FAM19A5 protein also affected depressive-like behaviors in mice. AAV9, a gene vector which shows the highest vector distribution throughout the central nervous system [35], was used to overexpress human FAM19A5 in the neurons of hippocampal CA1 region in naive C57BL/6 J mice (Fig. 3j). Since the C-terminal of *FAM19A5* gene expressed the Flag tag on AAV9 vector, we detected the expression of Flag and FAM19A5 in the hippocampus. As expected, mice that received AAV-FAM19A5 expressed strongly increased levels of FAM19A5 in hippocampus compared with those receiving a control AAV-Null (Supplementary Fig. S9A,

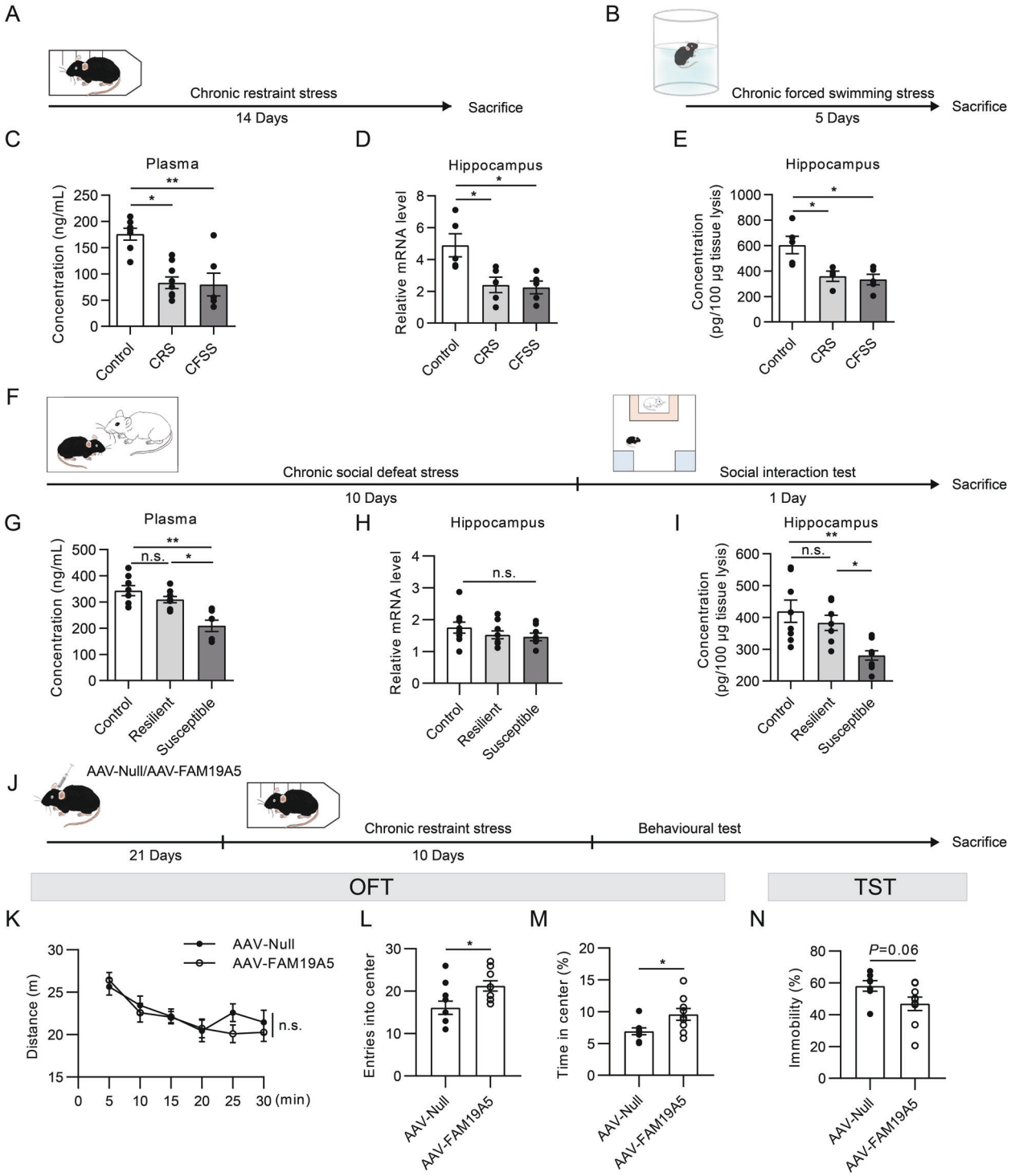

B). Using this approach, we next examined the consequences of FAM19A5 overexpression under chronic stress. Three weeks after virus injection, mice were subjected to CRS for another 10 days to induce depressive-like behaviors (Fig. 3j). There was no significant difference in the movement distance between CRS mice received AAV-FAM19A5 and controls within the total 30 min of the assessment in open field test, implying that FAM19A5 overexpression showed no significant effect on locomotor activity (Fig. 3k). Interestingly, we found a significant increase in the time spent in the center and the entries into the center of chamber elicited by FAM19A5 overexpression compared with the effects observed in mice that were injected with AAV-Null (Fig. 3l, m). We then performed

◀ **Fig. 3 Decreased FAM19A5 participated in the chronic stress-induced depression. a, b** Schematic illustration and timeline of chronic restraint stress (CRS) and chronic forced swimming stress (CFSS). **c** Cytometric bead measurements of plasma FAM19A5 from CRS- or CFSS-exposed mice ($n_{(Control,\ CRS,\ CFSS)} = 7, 9, 6$, one-way ANOVA with Dunn's multiple comparisons test, $P_{CRS} = 0.0116$, $P_{CFSS} = 0.0053$). **d** Quantitative real-time PCR (qPCR) detection of FAM19A5 mRNA expression levels in the hippocampus of CRS- or CFSS-exposed mice ($n = 5$ mice/group, one-way ANOVA with Dunn's multiple comparisons test, $P_{CRS} = 0.0294$, $P_{CFSS} = 0.0193$). **e** Cytometric bead detection of FAM19A5 protein expression levels in the hippocampus of CRS- or CFSS-exposed mice ($n = 5$ mice/group, one-way ANOVA with Dunn's multiple comparisons test, $P_{CRS} = 0.0323$, $P_{CFSS} = 0.0130$). **f** Schematic illustration and timeline of chronic social defeat stress (CSDS). **g** Cytometric bead measurements of plasma FAM19A5 from CSDS-exposed mice ($n_{(Control,\ Resilient,\ Susceptible)} = 8, 9, 7$, one-way ANOVA with Dunn's multiple comparisons test, control compared with susceptible: $P = 0.0010$, resilient compared with susceptible: $P = 0.0233$). **h** qPCR detection of FAM19A5 mRNA expression levels in the hippocampus of CSDS-exposed mice ($n_{(Control,\ Resilient,\ Susceptible)} = 9, 9, 8$, one-way ANOVA with Dunn's multiple comparisons test, control compared with susceptible: $P = 0.6329$, resilient compared with susceptible: $P > 0.9999$). **i** Cytometric bead detection of FAM19A5 protein expression levels in the hippocampus of CSDS-exposed mice ($n_{(Control,\ Resilient,\ Susceptible)} = 8, 7, 10$, one-way ANOVA with Dunn's multiple comparisons test, control compared with susceptible: $P = 0.0036$, resilient compared with susceptible: $P = 0.0246$). **j** Schematic of the experimental design of AAV9 overexpression treatment in mice subjected to chronic restraint stress. **k** Distance traveled during 5 min intervals in the open field test (two-way ANOVA with Sidak's multiple comparisons test; $P > 0.9999$). **l** Entries into the central zone (unpaired two-tailed Student's t test, $t = 2.513$, $P = 0.0223$) and **m** the percentage of time spent in the central zone (unpaired two-tailed Student's t test, $t = 2.376$, $P = 0.0312$) compared between mice infected with AAV-Null ($n = 8$) and AAV-FAM19A5 ($n = 9$). **n** The percentage of immobility time (unpaired two-tailed Student's t test, $t = 1.972$, $P = 0.0687$) compared between mice infected with AAV-Null ($n = 7$) and AAV-FAM19A5 ($n = 9$). All data are expressed as mean ± s.e.m.

tail suspension test and found that CRS mice received AAV-FAM19A5 exhibited less despair behaviors as indicated by decreased immobility during the test session than controls (Fig. 3n). Therefore, FAM19A5 overexpression in hippocampus could alleviate the chronic stress-induced depressive-like behaviors in mice.

Downregulation of AMPA receptors and NMDA receptors in the hippocampus of *Fam19a5*$^{-/-}$ mice

Since hippocampus has been shown to play a critical role in the phenotypes of depressive-like behavior and spatial memory impairment in *Fam19a5*$^{-/-}$ mice, we thus used RNA sequencing to capture transcriptome-wide alterations in the hippocampus of *Fam19a5*$^{-/-}$ mice and WT littermates. A comparison of differentially expressed genes between *Fam19a5*$^{-/-}$ mice and WT littermates within the hippocampus was presented by scatter plot (P adjust < 0.05, fold change >1.5) (Fig. 4a). To assess whether any particular biological pathway was associated with the dysregulated genes in *Fam19a5*$^{-/-}$ mice, we then applied KEGG analysis on the up- and downregulated gene sets. We found that "Neurodegenerative diseases," "Nervous system" and "Development" were the enriched categories when considering dysregulated genes in the hippocampus (Fig. 4b). Detection of differentially expressed genes in the hippocampus of *Fam19a5*$^{-/-}$ mice revealed the downregulation of α-amino-3-hydroxy-5-methyl-4-isoxazolepropionic acid (AMPA) receptors and N-methyl-D-aspartic acid (NMDA) receptors belong to "neuroactive ligand-receptor interaction" pathway, which is in agreement with the understanding that AMPA receptors and NMDA receptors signaling pathway plays an important role in modulating depression (Fig. 4c, d). We confirmed the downregulation of this glutamate receptor family using qPCR, indicating that the lack of FAM19A5 led to a significant downregulation of AMPA receptors and NMDA receptors in the hippocampus (Fig. 4e). Moreover, differentially expressed genes were functionally classified under broad categories on the basis of information from CellMarker Database [36] by using GSEA, which showed that differentially expressed genes were significantly enriched in neurons, progenitor cells and other cells, reflected in higher normalized enrichment score and more leading-edge genes (Fig. 4f).

Reduction of dendritic spine density, neuronal activity and glutamate release in *Fam19a5* deficiency mice

We sought to understand the underlying mechanism of FAM19A5 in regulating depressive-like behaviors and spatial memory impairment by examining whether FAM19A5 could affect the morphology of neuronal dendritic spines in mouse hippocampus. We found both immature spine (stubby and thin spine) and mature spine (mushroom spine) densities were significantly reduced in the hippocampus of *Fam19a5*$^{-/-}$ mice (Fig. 5a, b). Next, we used fiber photometry to monitor the calcium dynamics of the response of CA1 excitatory neurons to stimulation in the hippocampus. AAVs including rAAV-EF1α-DIO-GCaMP6s and rAAV-CaMKIIα-Cre were stereotaxically injected into the CA1 region of *Fam19a5*$^{-/-}$ mice and WT littermates (Fig. 5c). After 1 week following the viral infusion, we performed fiber photometry recordings of fluorescence during tail suspension test. During the immobility time of 5-min tail suspension test, Ca^{2+} signals of CA1 CaMKIIα^{+} neurons were significantly decreased in *Fam19a5*$^{-/-}$ mice (Fig. 5d, e), which was manifested by the significantly decreased frequency and amplitude of the recorded fluorescence signals (Fig. 5f). We then used iGluSnFR, a glutamate sensor to track endogenous glutamate dynamics in the mouse hippocampus, by injecting

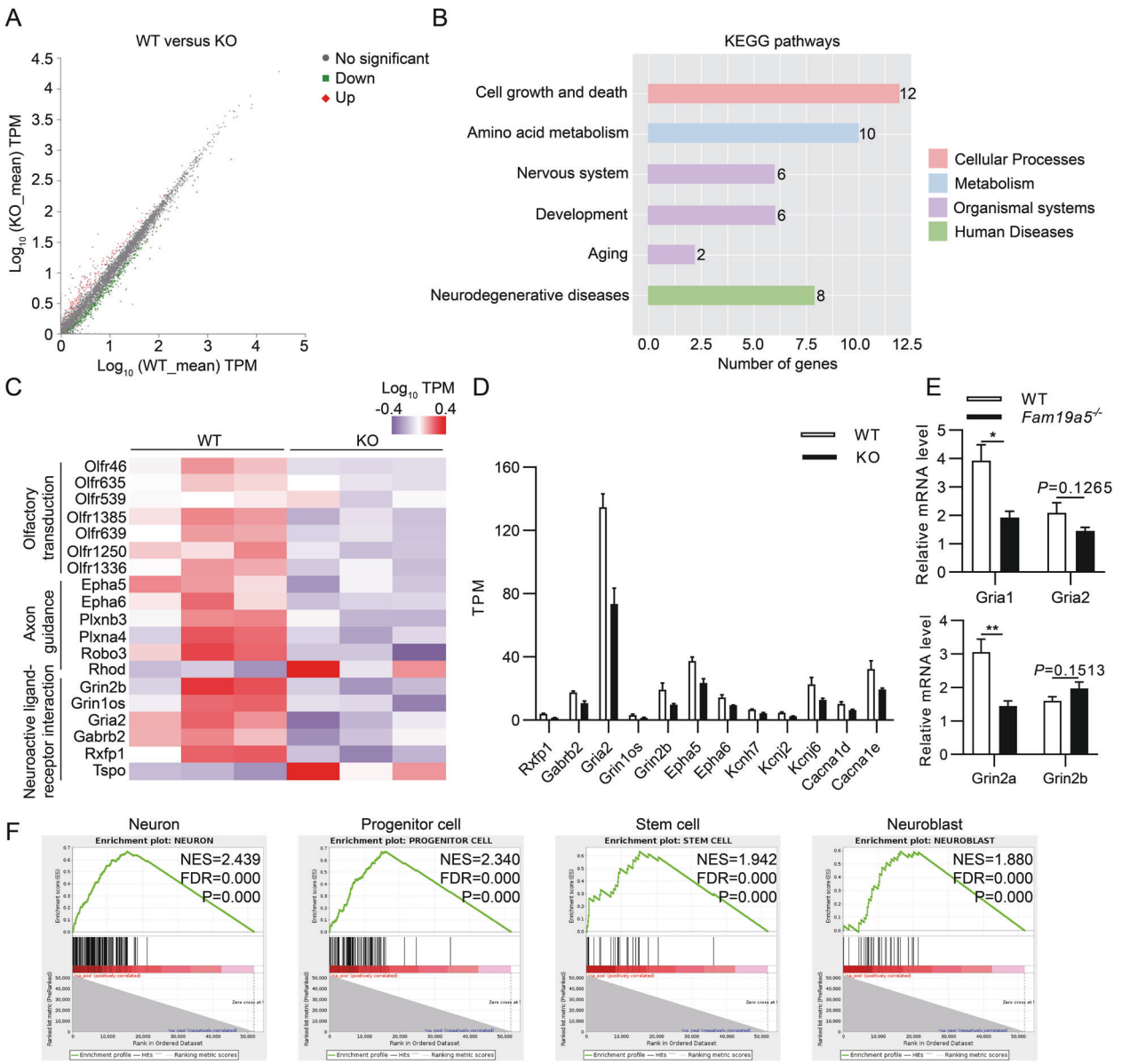

Fig. 4 Downregulation of AMPA receptors and NMDA receptors in the hippocampus of *Fam19a5*$^{-/-}$ mice. a Mean average plots comparing WT and KO mice RNA-seq data from hippocampus. Upregulated genes ($P < 0.05$) between WT and KO mice for each sample set were shown in red and downregulated genes ($P < 0.05$) were shown in green. WT and KO: $n = 3$. **b** Kyoto encyclopedia of genes and genomes (KEGG) pathway analysis of the differentially expressed (upregulated and downregulated) gene sets from the hippocampus ($P < 0.05$). The number of genes was displayed along the *x*-axis. **c** Heatmap for differentially expressed genes between WT and KO mouse hippocampus. **d** RNA-seq expression data of the significantly differentially expressed genes associated with some ion channels and receptors in the hippocampus. **e** RT-qPCR analysis verified the downregulation of Gria1, Gria2, Grin2a, Grin2b expression in the hippocampus (WT and KO: $n = 5$, unpaired two-tailed Student's *t* test, $^{*}P < 0.05$). **f** Gene set enrichment analysis (GSEA) analysis was performed on the differentially expressed genes from the hippocampus of WT and KO adult mice. Plot showed the running sum of enrichment score (ES) for ranked genes comparing with the neurocyte gene sets. Gene sets with a normalized enrichment score (NES) > 2 and a false discovery rate (FDR) of <0.05 were considered significant. All data are expressed as mean ± s.e.m.

rAAV-EF1α-DIO-iGluSnFR(A184S) and rAAV-CaMKIIα-Cre into CA1 of *Fam19a5*$^{-/-}$ mice and WT littermates. The fluorescence signals were increased continuously in WT mice suspended by the tail, while the signals showed a steady decline in *Fam19a5*$^{-/-}$ mice (Fig. 5g, h). The area under the curve of the fluorescence signals in *Fam19a5*$^{-/-}$ mice decreased significantly compared with WT littermates (Fig. 5i). All recording sites were confirmed post hoc within the CA1 (Supplementary Fig. S10A, B). Taken together, these results suggested that *Fam19a5*$^{-/-}$ mice exhibited a reduction of dendritic spine density as well as neuronal activity and glutamate release.

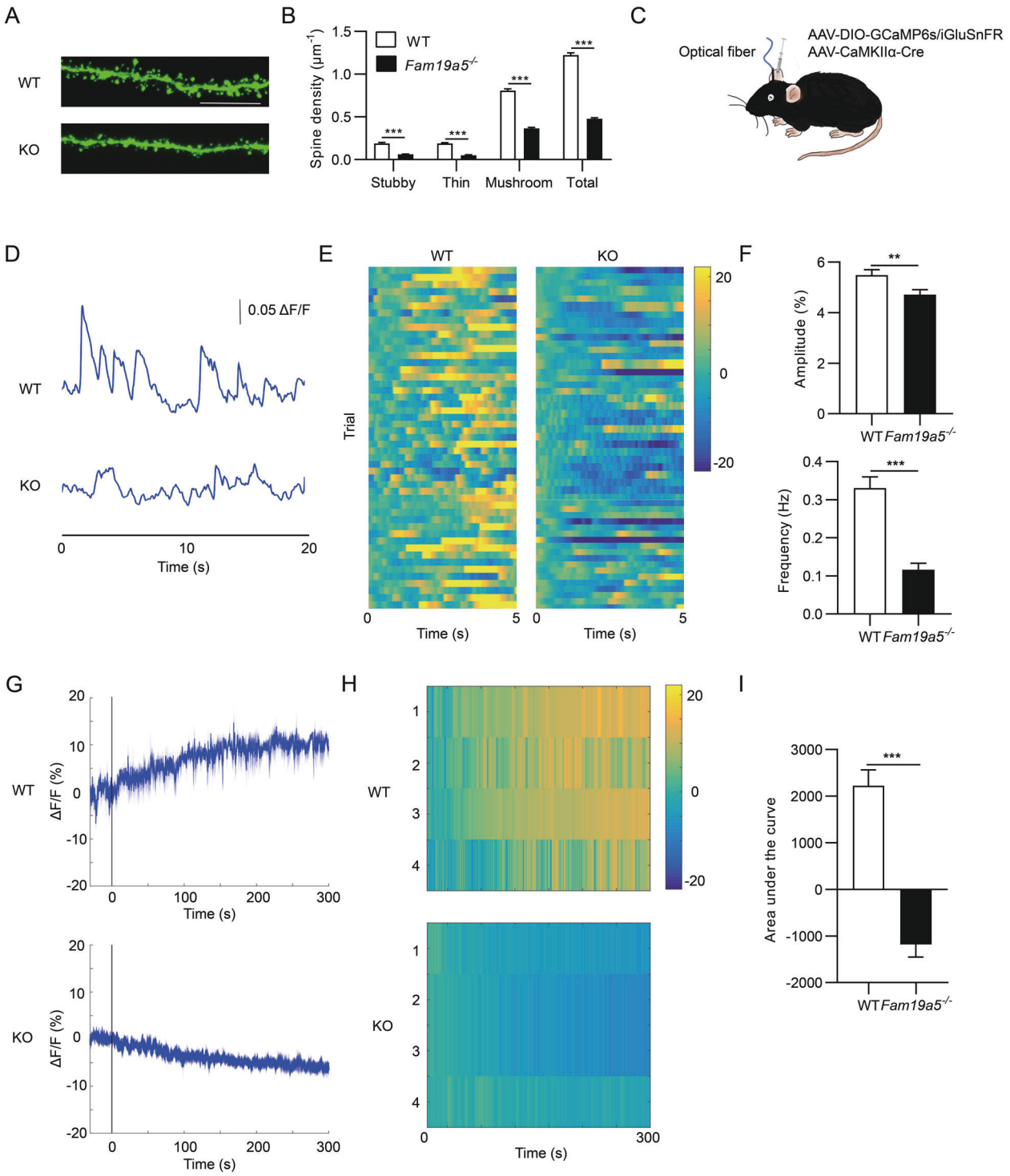

Discussion

Previously, we have shown that FAM19A5 is highly expressed in adipose tissue [7]. In this study, we provided several lines of evidence showing that FAM19A5 was abundantly expressed in the hippocampus, in which it was particularly expressed in glutamatergic neurons, while moderately expressed within other regions of adult mice brain, consistent with a recent research [5], indicating that FAM19A5 was not only an adipokine but also a neurokine. A previous meta-analysis of diagnostic and intervention studies has suggested that adipokines are involved in the pathophysiology of depression and can act as emerging depression biomarkers [37]. A recent research has also

◀ **Fig. 5 Reduction of dendritic spine density, neuronal activity and glutamate release in *Fam19a5* deficiency mice. a** Representative images of dendrite segments of CA1 pyramidal neurons from WT and KO mice. Scale bar, 10 μm. **b** The densities of total, mushroom, stubby and thin dendritic spines in *Fam19a5*$^{-/-}$ mice compared with WT littermates (WT: 120 dendritic spines from 3 mice, KO: 138 dendritic spines from 4 mice, two-way ANOVA with Sidak's multiple comparisons test, ***$P < 0.001$). **c–f** Ca^{2+} signals recorded from CA1 CaMKIIα^{+} neurons. **c** Schematic diagram depicting the virus injection and fiber photometry recording. **d** Peri-event plots of the average Ca^{2+} transients from representative WT and *Fam19a5*$^{-/-}$ mice. **e** Heatmap illustration of Ca^{2+} signals aligned to the immobility time of tail suspension was shown for both WT and *Fam19a5*$^{-/-}$ mice. Each row represented Ca^{2+} signal changes during one episode of immobility. Color scale indicated the range of ΔF/F. **f** Amplitude (WT: $n = 3$, KO: $n = 3$, unpaired two-tailed Student's t test, $t = 2.607$, $P = 0.0098$) and frequency (unpaired two-tailed Student's t test, $t = 6.358$, $P < 0.001$) of activation of CA1 CaMKIIα^{+} neurons. **g–i** Glutamate dynamics recorded from CA1 CaMKIIα^{+} neurons in WT and *Fam19a5*$^{-/-}$ mice. **g** Peri-event plots of the average glutamate transients from representative WT and *Fam19a5*$^{-/-}$ mice. Thick lines indicated mean, and shaded areas indicated s.e.m. **h** Heatmap illustration of glutamate signals aligned to the tail suspension was shown for both WT and *Fam19a5*$^{-/-}$ mice. Color scale indicated the range of ΔF/F. **i** Area under the curve of glutamate release of CA1 CaMKIIα^{+} neurons (WT: $n = 4$, KO: $n = 4$, unpaired two-tailed Student's t test, $t = 7.878$, $P = 0.0002$). All data are expressed as mean ± s.e.m.

found that adipokines may either predict response to ketamine or act as possible transducers of its therapeutic effects in depression [38]. Here, we showed that FAM19A5, which acts as not only an adipokine but a neurokine and abundantly expressed in the brain, could be used as an indicator of vulnerability to stress-induced disorders.

The role of FAM19A5 was illustrated by the facts that the ablation of FAM19A5 led to depressive-like behaviors and cognitive impairment in mice. *Fam19a5*$^{-/-}$ mice exhibited anhedonia revealed by less appetite for sucrose and more depressive-like behaviors reflected by increased immobility in forced swimming test and tail suspended test. Moreover, we observed that loss of FAM19A5 substantially caused impaired hippocampus-dependent spatial memory, as demonstrated by significant increased time to find the platform during training phase, significant reduced time spent in the target quadrant and number of crossing the target platform position during the probe phase in the MWM test. Interestingly, *Fam19a5*$^{-/-}$ mice showed an increased locomotor activity reflected by open field test, which probably displayed abnormal hyperactivity or anxiety-like behavior. However, the deficiency of FAM19A5 had no effect on anxiety-related behavior in mice. These results suggested that, although FAM19A5 was widely expressed in various brain regions, the absence of FAM19A5 may lead to specific abnormal behaviors especially depression and cognitive impairment.

Emerging evidence has shown that chronic stress is a potent causal factor for eliciting major depressive disorder (MDD) and has an important effect on hippocampal functions [39, 40]. To investigate whether FAM19A5 contributed to the chronic stress-induced depression, we examined alterations of FAM19A5 in both plasma and hippocampus in mouse models of chronic stress. Our results showed that the circulating FAM19A5 levels were reduced in mice exposed to CRS or CFSS, and in susceptible mice exposed to CSDS, while remained unchanged in resilient mice exposed to CSDS. Consistently, a reduction of FAM19A5 level was also found in hippocampus but not in amygdala and hypothalamus in these mouse models of chronic stress-induced depression, indicating the involvement of hippocampal FAM19A5 in the development of depression. Furthermore, overexpressing FAM19A5 in the hippocampus of CRS mice by AAV9 vectors could attenuate the CRS-induced depressive-like behaviors, indicating that FAM19A5 may be a key factor involved in depressive-like behavior and mediate antidepressant-like effects in mice subjected to chronic stress. Selective serotonin reuptake inhibitors (SSRIs) are a widely used class of antidepressants, but SSRIs generally take several weeks to exert antidepressant effects [41]. Ketamine, as a rapid and sustained antidepressant, has several drawbacks such as neurotoxicity and abuse potential [42]. Therefore, it is urgent to explore new antidepressant targets. In view of our current results, we suggested that FAM19A5 may be a promising biomarker of vulnerability to depression and a potential therapeutic target for depression.

It is well established that the modulation of synaptic plasticity participates in hippocampal functions such as learning and memory, anxiety, and emotion regulation [43]. Indeed, the decreased synaptic function has been found in depression condition [18, 44]. For example, it has been specified that chronic stress consistently leads to the dysregulation of glutamate signaling and decrease in synapse density and diameter [44–47]. In this study, we actually observed a reduction of dendritic spine density in the hippocampal neurons of *Fam19a5*$^{-/-}$ mice, validating the role of FAM19A5 in the regulation of synaptic plasticity. Moreover, we demonstrated that the levels of ionotropic glutamate receptors including AMPA receptors and NMDA receptors and many other ion channels that participate in synaptic transmission and neuronal excitability, were decreased in *Fam19a5*$^{-/-}$ mice. We also demonstrated that the reduction of AMPA receptors and NMDA receptors caused the reduction of neuronal activity in *Fam19a5*$^{-/-}$ mice. Chronic stress has been shown to affect the availability of synaptic AMPA receptors and NMDA receptors as well as the density and diameter of neuronal dendritic spines, and the extracellular glutamate clearance by glial cells in the cortex and hippocampus [18]. These microstructural and molecular changes are thought to underlie several abnormalities observed in the brains of MDD

patients, including changes in glutamate levels and altered function and connectivity within brain networks [48, 49]. In addition, glutamatergic synaptic plasticity and changes in synaptic connectivity have also been shown to be essential to learning and memory [50, 51]. Glutamate system has been proved to involve in spine formation and the functional significance of new spines to neuronal connectivity [52]. These results implied the possible roles of FAM19A5 deficiency in the development of depression and cognitive impairment in mice. Under normal conditions, glutamate transmission is balanced and optimized to provide high signal-to-noise ratio and integrity of signal transfer [53]. In *Fam19a5* deficiency mice, reduction of glutamate neurotransmitter system including decrease in glutamate release and the expression of postsynaptic ionotropic glutamate receptors would result in the degradation of signal integrity in the hippocampus. Subsequently, these changes led to the atrophy of glutamatergic neurons, such as the decreased density of dendrite spines, which ultimately brought about changes in behaviors.

In summary, we provided several lines of evidence showing that FAM19A5 was highly expressed in the brain especially in the hippocampus. We further discovered that FAM19A5 was expressed in neurons, oligodendrocytes and NSCs. FAM19A5 was decreased in plasma and hippocampus in mice subjected to chronic stress. We addressed the protective role of human FAM19A5 in chronic stress. *Fam19a5*$^{-/-}$ mice displayed increased depressive-like behaviors and spatial memory impairment. Moreover, we found that FAM19A5 also played an essential role in maintaining the density and morphology of dendritic spines, neuronal activity and glutamate transmission in the hippocampus. Our present data raised the possibility of FAM19A5 as a promising biomarker and a potential therapeutic target for depression, and provided a new mechanism for chronic stress-induced depression.

Acknowledgements This work was supported by National Natural Science Foundation of China (81970536, 81974169, 31770940, 61527815 and 81671085), Natural Science Foundation of Beijing Municipality (7192097) and the Non-profit Central Research Institute Fund of Chinese Academy of Medical Sciences (2019PT320006). We are grateful to Professor Dalong Ma (Department of Immunology, School of Basic Medical Sciences, NHC Key Laboratory of Medical Immunology and Center for Human Disease Genomics, Peking University) for his omics strategies and valuable suggestions.

Author contributions YW (Ying Wang), GGX (Guo-Gang Xing), and SYH conceived the project, designed the experiments and wrote the manuscript. SYH, CZ, and GGX (Guoguang Xie) performed most of the experiments. ZMS, DXC, YZ, WWL, SPS, QQL, and ZTL performed some experiments or analyzed the data. PZW provided help for the bioinformatics analysis. PL provided help for prepared polyclonal antibodies. YB provided a few important advices for the work. YW (Yun Wang) provided behavioral experimental facilities. All authors have discussed the results and contributed to the drafting of the manuscript.

Compliance with ethical standards

Conflict of interest The authors declare that they have no conflict of interest.

Publisher's note Springer Nature remains neutral with regard to jurisdictional claims in published maps and institutional affiliations.

References

1. Tom Tang Y, Emtage P, Funk WD, Hu T, Arterburn M, Park EE, et al. TAFA: a novel secreted family with conserved cysteine residues and restricted expression in the brain. Genomics. 2004;83:727–34.
2. Lei X, Liu L, Terrillion CE, Karuppagounder SS, Cisternas P, Lay M, et al. FAM19A1, a brain-enriched and metabolically responsive neurokine, regulates food intake patterns and mouse behaviors. FASEB J. 2019;33:14734–47.
3. Wang X, Shen C, Chen X, Wang J, Cui X, Wang Y, et al. Tafa-2 plays an essential role in neuronal survival and neurobiological function in mice. Acta biochimica et biophysica Sin. 2018;50:984–95.
4. Paulsen SJ, Christensen MT, Vrang N, Larsen LK. The putative neuropeptide TAFA5 is expressed in the hypothalamic paraventricular nucleus and is regulated by dehydration. Brain Res. 2008;1199:1–9.
5. Shahapal A, Cho EB, Yong HJ, Jeong I, Kwak H, Lee JK, et al. FAM19A5 expression during embryogenesis and in the adult traumatic brain of FAM19A5-LacZ knock-in mice. Front Neurosci. 2019;13:917.
6. Kashevarova AA, Belyaeva EO, Nikonov AM, Plotnikova OV, Skryabin NA, Nikitina TV, et al. Compound phenotype in a girl with r(22), concomitant microdeletion 22q13.32-q13.33 and mosaic monosomy 22. Mol Cytogenetics. 2018;11:26.
7. Wang Y, Chen D, Zhang Y, Wang P, Zheng C, Zhang S, et al. Novel adipokine, FAM19A5, inhibits neointima formation after injury through sphingosine-1-phosphate receptor 2. Circulation. 2018;138:48–63.
8. Akahoshi N, Ishizaki Y, Yasuda H, Murashima YL, Shinba T, Goto K, et al. Frequent spontaneous seizures followed by spatial working memory/anxiety deficits in mice lacking sphingosine 1-phosphate receptor 2. Epilepsy Behav. 2011;22:659–65.
9. Fanselow MS, Dong HW. Are the dorsal and ventral hippocampus functionally distinct structures? Neuron. 2010;65:7–19.
10. MacQueen G, Frodl T. The hippocampus in major depression: evidence for the convergence of the bench and bedside in psychiatric research? Mol Psychiatry. 2011;16:252–64.
11. Bird CM, Burgess N. The hippocampus and memory: insights from spatial processing. Nat Rev Neurosci. 2008;9:182–94.
12. Rottenberg J. Emotions in depression what do we really know. Annu Rev Clin Psychol. 2017;13:241–63.
13. Krishnan V, Nestler EJ. The molecular neurobiology of depression. Nature. 2008;455:894–902.
14. Nestler EJ, Barrot M, DiLeone RJ, Eisch AJ, Gold SJ, Monteggia LM. Neurobiology of depression. Neuron. 2002;34:13–25.
15. Pena CJ, Bagot RC, Labonte B, Nestler EJ. Epigenetic signaling in psychiatric disorders. J Mol Biol. 2014;426:3389–412.
16. Gold PW. The organization of the stress system and its dysregulation in depressive illness. Mol Psychiatry. 2015;20:32–47.

17. Park C, Rosenblat JD, Brietzke E, Pan Z, Lee Y, Cao B, et al. Stress, epigenetics and depression: a systematic review. Neurosci Biobehav Rev. 2019;102:139–52.
18. Popoli M, Yan Z, McEwen BS, Sanacora G. The stressed synapse: the impact of stress and glucocorticoids on glutamate transmission. Nat Rev Neurosci. 2011;13:22–37.
19. Aston-Jones G, Cohen JD. An integrative theory of locus coeruleus-norepinephrine function adaptive gain and optimal performance. Annu Rev Neurosci. 2005;28:403–50.
20. Raison CL, Capuron L, Miller AH. Cytokines sing the blues: inflammation and the pathogenesis of depression. Trends Immunol. 2006;27:24–31.
21. McIntyre C, Saville J, Fuller M. Collection of cerebrospinal fluid from murine lateral ventricles for biomarker determination in mucopolysaccharidosis type IIIA. J Neurosci Methods. 2019;324:108314.
22. Zheng C, Chen D, Zhang Y, Bai Y, Huang S, Zheng D, et al. FAM19A1 is a new ligand for GPR1 that modulates neural stem-cell proliferation and differentiation. FASEB J. 2018;32: 5874–90.
23. Jaworski J, Kapitein LC, Gouveia SM, Dortland BR, Wulf PS, Grigoriev I, et al. Dynamic microtubules regulate dendritic spine morphology and synaptic plasticity. Neuron. 2009;61:85–100.
24. Angelova PR, Kasymov V, Christie I, Sheikhbahaei S, Turovsky E, Marina N, et al. Functional oxygen sensitivity of astrocytes. J Neurosci. 2015;35:10460–73.
25. Kasymov V, Larina O, Castaldo C, Marina N, Patrushev M, Kasparov S, et al. Differential sensitivity of brainstem versus cortical astrocytes to changes in pH reveals functional regional specialization of astroglia. J Neurosci. 2013;33:435–41.
26. Kim KS, Han PL. Optimization of chronic stress paradigms using anxiety- and depression-like behavioral parameters. J Neurosci Res. 2006;83:497–507.
27. Yang Y, Cui Y, Sang K, Dong Y, Ni Z, Ma S, et al. Ketamine blocks bursting in the lateral habenula to rapidly relieve depression. Nature. 2018;554:317–22.
28. Krishnan V, Han MH, Graham DL, Berton O, Renthal W, Russo SJ, et al. Molecular adaptations underlying susceptibility and resistance to social defeat in brain reward regions. Cell. 2007;131: 391–404.
29. Young P, Qiu L, Wang D, Zhao S, Gross J, Feng G. Single-neuron labeling with inducible Cre-mediated knockout in transgenic mice. Nat Neurosci. 2008;11:721–8.
30. Xiong R, Verstraelen P, Demeester J, Skirtach AG, Timmermans JP, De Smedt SC, et al. Selective labeling of individual neurons in dense cultured networks with nanoparticle-enhanced photoporation. Front Cell Neurosci. 2018;12:80.
31. Li Y, Zhong W, Wang D, Feng Q, Liu Z, Zhou J, et al. Serotonin neurons in the dorsal raphe nucleus encode reward signals. Nat Commun. 2016;7:10503.
32. Marvin JS, Scholl B, Wilson DE, Podgorski K, Kazemipour A, Muller JA, et al. Stability, affinity, and chromatic variants of the glutamate sensor iGluSnFR. Nat Methods. 2018;15:936–9.
33. Anacker C, Hen R. Adult hippocampal neurogenesis and cognitive flexibility—linking memory and mood. Nat Rev Neurosci. 2017;18:335–46.
34. Henn FA, Vollmayr B. Stress models of depression: forming genetically vulnerable strains. Neurosci Biobehav Rev. 2005;29:799–804.
35. Cearley CN, Wolfe JH. Transduction characteristics of adeno-associated virus vectors expressing cap serotypes 7, 8, 9, and Rh10 in the mouse brain. Mol Ther. 2006;13:528–37.
36. Zhang X, Lan Y, Xu J, Quan F, Zhao E, Deng C, et al. CellMarker: a manually curated resource of cell markers in human and mouse. Nucleic Acids Res. 2019;47:D721–8.
37. Carvalho AF, Rocha DQ, McIntyre RS, Mesquita LM, Kohler CA, Hyphantis TN, et al. Adipokines as emerging depression biomarkers: a systematic review and meta-analysis. J Psychiatr Res. 2014;59:28–37.
38. Machado-Vieira R, Gold PW, Luckenbaugh DA, Ballard ED, Richards EM, Henter ID, et al. The role of adipokines in the rapid antidepressant effects of ketamine. Mol Psychiatry. 2017;22:127–33.
39. Hammen C. Stress and depression. Annu Rev Clin Psychol. 2005;1:293–319.
40. Wingenfeld K, Wolf OT. Stress, memory, and the hippocampus. Front Neurol Neurosci. 2014;34:109–20.
41. Berton O, Nestler EJ. New approaches to antidepressant drug discovery: beyond monoamines. Nat Rev Neurosci. 2006;7: 137–51.
42. Chaki S. Beyond ketamine: new approaches to the development of safer antidepressants. Curr Neuropharmacol. 2017;15:963–76.
43. Leuner B, Gould E. Structural plasticity and hippocampal function. Annu Rev Psychol. 2010;61:111–40. C111-113.
44. Murrough JW, Abdallah CG, Mathew SJ. Targeting glutamate signalling in depression: progress and prospects. Nat Rev Drug Discov. 2017;16:472–86.
45. Li MX, Zheng HL, Luo Y, He JG, Wang W, Han J, et al. Gene deficiency and pharmacological inhibition of caspase-1 confers resilience to chronic social defeat stress via regulating the stability of surface AMPARs. Mol Psychiatry. 2018;23:556–68.
46. Thompson SM, Kallarackal AJ, Kvarta MD, Van Dyke AM, LeGates TA, Cai X. An excitatory synapse hypothesis of depression. Trends Neurosci. 2015;38:279–94.
47. Duman RS, Aghajanian GK, Sanacora G, Krystal JH. Synaptic plasticity and depression: new insights from stress and rapid-acting antidepressants. Nat Med. 2016;22:238–49.
48. Yuksel C, Ongur D. Magnetic resonance spectroscopy studies of glutamate-related abnormalities in mood disorders. Biol Psychiatry. 2010;68:785–94.
49. Kaiser RH, Andrews-Hanna JR, Wager TD, Pizzagalli DA. Large-scale network dysfunction in major depressive disorder: a meta-analysis of resting-state functional connectivity. JAMA Psychiatry. 2015;72:603–11.
50. Bliss TV, Collingridge GL. A synaptic model of memory long-term potentiation in the hippocampus. Nature. 1993;361:31–39.
51. Kessels HW, Malinow R. Synaptic AMPA receptor plasticity and behavior. Neuron. 2009;61:340–50.
52. Kwon HB, Sabatini BL. Glutamate induces de novo growth of functional spines in developing cortex. Nature. 2011;474:100–4.
53. Duman RS, Sanacora G, Krystal JH. Altered connectivity in depression: GABA and glutamate neurotransmitter deficits and reversal by novel treatments. Neuron. 2019;102:75–90.